Novel microfabrication stage allowing for one-photon and multi-photon Light Assisted Molecular Immobilization and for multi-photon microscope

Gonçalves, Odete; Snider, Scott; Zadoyan, Ruben; Nguyen, Quoc Thang; Vorum, Henrik; Petersen, Steffen B.; Neves-Petersen, Maria Teresa

Published in:
Reporters, Markers, Dyes, Nanoparticles, and Molecular Probes for Biomedical Applications IX, SPIE BiOS, 28 January - 2 February 2017, San Francisco, CA, USA

DOI (link to publication from Publisher):
10.1117/12.2250567

Publication date:
2017

Document Version
Publisher's PDF, also known as Version of record

PROCEEDINGS OF SPIE

SPIEDigitalLibrary.org/conference-proceedings-of-spie

Novel microfabrication stage allowing for one-photon and multi-photon light assisted molecular immobilization and for multi-photon microscope

Odete Gonçalves, Scott Snider, Ruben Zadoyan, Quoc-Thang Nguyen, Henrik Vorum, et al.

Odete Gonçalves, Scott Snider, Ruben Zadoyan, Quoc-Thang Nguyen, Henrik Vorum, Steffen B. Petersen, Maria Teresa Neves-Petersen, "Novel microfabrication stage allowing for one-photon and multi-photon light assisted molecular immobilization and for multi-photon microscope," Proc. SPIE 10079, Reporters, Markers, Dyes, Nanoparticles, and Molecular Probes for Biomedical Applications IX, 100790F (21 February 2017); doi: 10.1117/12.2250567

SPIE.

Event: SPIE BiOS, 2017, San Francisco, California, United States

Novel microfabrication stage allowing for one-photon and multi-photon Light Assisted Molecular Immobilization and for multi-photon microscope

Odete Gonçalves [a], Scott Snider [b], Ruben Zadoyan [b], Quoc-Thang Nguyen [†c], Henrik Vorum [d], Steffen B. Petersen [a], Maria Teresa Neves-Petersen*[d]

[a] Department of Health Science and Technology, Aalborg University, Fredrik Bajers vej 7, DK-9220, Aalborg, Denmark
[b] Newport Corporation, Technology & Applications Center, 1791 Deere Avenue, Irvine, CA 92606, United States of America
[c] NeurAccel Biosciences, 11099 North Torrey Pines, La Jolla, CA 92037, United States of America
[d] Department of Clinical Medicine, Aalborg University, Søndre Skovvej 15, DK-9000, Aalborg, Denmark

ABSTRACT

Light Assisted Molecular Immobilization (LAMI) results in spatially oriented and localized covalent coupling of biomolecules onto thiol reactive surfaces. LAMI is possible due to the conserved spatial proximity between aromatic residues and disulfide bridges in proteins. When aromatic residues are excited with UV light (275-295nm), disulphide bridges are disrupted and the formed thiol groups covalently bind to surfaces. Immobilization hereby reported is achieved in a microfabrication stage coupled to a fs-laser, through one- or multi-photon excitation. The fundamental 840nm output is tripled to 280nm and focused onto the sample, leading to one-photon excitation and molecular immobilization. The sample rests on a xyz-stage with micrometer step resolution and is illuminated according to a pattern uploaded to the software controlling the stage and the shutter. Molecules are immobilized according to such pattern, with micrometer spatial resolution. Spatial masks inserted in the light path lead to light diffraction patterns used to immobilize biomolecules with submicrometer spatial resolution. Light diffraction patterns are imaged by an inbuilt microscope. Two-photon microscopy and imaging of the fluorescent microbeads is shown.

Immobilization of proteins, e.g. C-reactive protein, and of an engineered molecular beacon has been successfully achieved. The beacon was coupled to a peptide containing a disulfide bridge neighboring a tryptophan residue, being this way possible to immobilize the beacon on a surface using one-photon LAMI. This technology is being implemented in the creation of point-of-care biosensors aiming at the detection of cancer and cardiovascular disease markers.

Keywords: Light Assisted Molecular Immobilization (LAMI), Biosensor, Photonic immobilization, microfabrication stage, C-reactive protein, Molecular Beacon, one-photon and multi-photon excitation.

1. INTRODUCTION

Biomarker detection is of great importance in, e.g., medicine, the food industry and environmental analysis. Immobilization of biomolecules onto biosensor structures has been widely implemented. Molecules can be immobilized to a surface in a covalent or non-covalent way[1]. The risk of altering the structure and therefore the recognition ability of the immobilized biosensors increases for protocols with a larger number of chemical steps. Furthermore, most of the commonly used methods achieve immobilization of the biosensors in a random spatial orientation which might lead to a decrease in biorecognition of target analytes[2].

*nevespetersen@gmail.com Phone: +45 22522475 †Deceased February 11, 2016

Reporters, Markers, Dyes, Nanoparticles, and Molecular Probes for Biomedical Applications IX
edited by Samuel Achilefu, Ramesh Raghavachari, Proc. of SPIE Vol. 10079, 100790F

Light Assisted Molecular Immobilization (LAMI) is a photonic technology that leads to covalent and oriented immobilization of biomolecules onto sensor surfaces [3–6], with no need to expose the sensor biomolecule to chemicals or thermal steps. The immobilized biomolecules remain active. In the present paper, we describe in detail a new microfabrication stage that has been built in order to implement LAMI, using one-photon or multi-photon excitation. LAMI involves the breakage of disulphide bonds upon UV illumination of nearby aromatic residues, creating free thiol groups that can covalently bind to a thiol reactive surface (Figure 1). The spatial proximity between aromatic residues to disulphide bridges is a conserved motif in proteins[7].

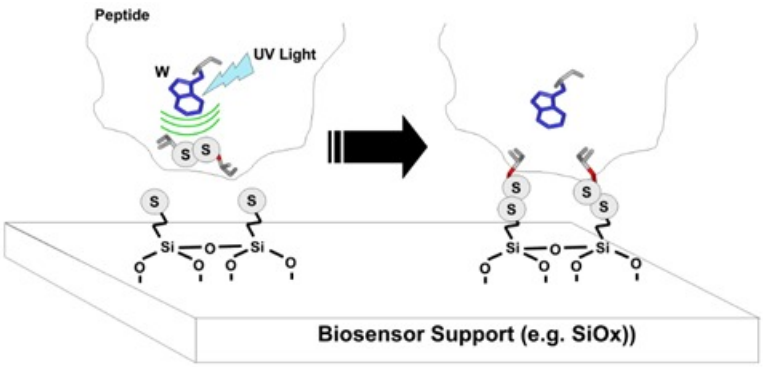

Figure 1. UV excitation of an aromatic residue (Trp, W) in the peptide will lead to the disruption of the nearby disulphide bridge, leading to the formation of free SH groups. Afterwards, these groups will covalently bind to the free thiol groups present on the biosensor support (e.g. SiOx). (adapted from [8])

The side chains of Tryptophan (Trp), Tyrosine (Tyr) and Phenylalanine (Phe) absorb UV light. Trp and Tyr are the best absorbers, displaying an absorbance peak at 280nm. They are excited to higher energy states, with subsequent relaxation to the ground state or they can undergo photochemical processes such as photoionization. The light induced ejected electron will be caged by water molecules, leading to the formation of a solvated electron (e^-_{aq}) (scheme 1), which reacts with a nearby disulphide bridge forming a disulphide electron adduct (see schemes 5 and 9). The adduct can also be formed when the disulphide bridges react with the triplet states of Trp or Tyr residues (schemes 5 and 9). The formation of one such triplet spin states is illustrated in schemes 3 and 4. The adduct easily dissociates leading to a broken disulphide bridge (schemes 11 and 12).

After excitation, Trp may undergo a non-radiative relaxation channel, leading to the formation of solvated electrons and yielding a neutral radical $Trp^{\bullet}$ resulting from the $Trp^{\bullet+}$ radical cation (schemes 1 and 2). It may also lead to the disruption of nearby disulphide bridges if the excited Trp undergoes intersystem crossing, yielding the triplet state ^3Trp which can, in turn, transfer an electron to a nearby disulphide bridge, giving rise to a tryptophan radical cation and the disulphide bridge electron adduct $RSSR^{\bullet-}$ (schemes 3-5).

$$Trp + h\nu \rightarrow Trp^{\bullet+} + e^-_{aq} \quad (1)$$

$$Trp^{\bullet+} \rightarrow Trp^{\bullet} + H^+ \quad (2)$$

$$^1Trp + h\nu \rightarrow {}^1Trp^* \quad (3)$$

$$^1Trp^* \rightarrow {}^3Trp \quad (4)$$

$$^3Trp + RSSR \rightarrow Trp^{\bullet+} + RSSR^{\bullet-} \quad (5)$$

Tyr may also undergo non-radiative decay, fluoresce, or undergo intersystem crossing to the triplet state. It can also be photoionized, at neutral pH, by absorbing a second photon from the triplet state leading to the formation of a solvated electron (e^-_{aq}) (scheme 6). This will give rise to a neutral radical $Tyr\text{-}OH^{\bullet}$ that results from the rapid deprotonation of the

radical cation Tyr-OH$^{\bullet+}$ (scheme 7) and to a solvated electron (e^-_{aq}). The neutral radical Tyr-O$^{\bullet}$ may also result from photoionization of tyrosinate at high pH, also giving rise to a solvated electron (e^-_{aq}) (scheme 8).

$$^3Tyr-OH + h\nu \rightarrow Tyr-OH^{\bullet+} + e^-_{aq} \quad (6)$$

$$Tyr-OH^{\bullet+} \rightarrow Tyr-OH^{\bullet} + H^+ \quad (7)$$

$$Tyr-O^{\bullet-} + h\nu \rightarrow Tyr-O^{\bullet} + e^-_{aq} \quad (8)$$

A nearby Trp or disulphide bridge rapidly quenches the triplet state of Tyr, according to [3]:

$$^3Tyr-OH + RSSR \rightarrow Tyr-O^{\bullet} + H^+ + RSSR^{\bullet-} \quad (9)$$

One photochemical process that enables LAMI involves the reduction of SS bridges upon UV excitation of Tyr and/or Trp [9,10]. The solvated electrons that can result from the UV excitation of these aromatic residues can be captured by electrophilic species, such as cystines. The breakage of the SS bridges results as a consequence of the electron capture by the cystine:

$$e^-_{aq} + RSSR \rightarrow RSSR^{\bullet-} \quad (10)$$

$$RSSR^{\bullet-} \Leftrightarrow RS^{\bullet} + RS^- \quad (11)$$

$$RSSR^{\bullet-} + H^+ \Leftrightarrow RS^{\bullet} + RSH \quad (12)$$

Previous work by Neves-Petersen et al. has demonstrated the reduction of SS bridges upon UV excitation of the aromatic pool in various proteins such as lysozyme and cutinase [8,10], prostate specific antigen[7], bovine serum albumin[6,11], insulin[12], alpha-lactalbumin[13], plasminogen[14] and antibody Fab fragments[15]. Protein immobilization with submicrometer spatial resolution was also demonstrated in previous works using LAMI. Spatial masks were used to obtain these patterns. The spatial masks were placed before the focusing lens prior to the protein sample. Such masks created a light diffraction pattern which led to protein immobilization[5,6]. With the previous optical setup used by the group, it was possible to image the submicrometer spatially resolved protein fluorescent patterns but not the light diffraction patterns that led to protein immobilization.

In this paper, we report new molecular models immobilized with LAMI technology using an improved customized optical setup designed and built in partnership with Newport Corporation. The new optical setup presents a series of improvements regarding the previously described optical setup to carry on LAMI[5,6]. It allows imaging of the light diffraction patterns formed by the spatial masks through a windowless CCD camera placed above the objectives. By observing these patterns, it is possible to make a match between the formed light patterns and the obtained immobilized patterns, which was not possible with the previous setup. This new setup also allows for multiphoton excitation. It is possible to image samples with two- or three-photon excitation and to immobilize biomolecules through three-photon excitation, using the IR pathway. Through the UV pathway, it is possible to immobilize biomolecules through one-photon excitation.

The new features of the illumination setup allow for new applications of LAMI, being possible to obtain immobilized biosensors through one- and three-photon excitation. It also allows for two- and three-photon confocal microscopy and the visualization of light patterns, due to the CCD camera installed above the illumination setup.

2. MATERIAL AND METHODS

2.1. Protein and Buffer Solutions

C-reactive protein (CRP) was kindly provided by the Universitat Politècnica de València (UPV) (Sigma product C1617). CRP was conjugated with Alexa Fluor 647. CRP concentration was 109 µg/mL (4.3 µM protomer, 0.87 µM pentamer) in 1x PBS buffer. The molecular beacon (MB) coupled to a fluorescent probe (Cy3) and a quencher molecule (DABCYL) and the complementary oligonucleotide were produced and purchased from Biosynthesis (Texas, USA). The lyophilized MB and complementary oligonucleotide were dissolved in PBS 1x to a final concentration of 10µM.

2.2. Protein 3D structure and engineered Molecular Beacon construct

2.2.1 Molecular Beacon (MB)

The structure of the model MB is depicted in Figure 3. The model MB structure consists of an oligonucleotide with the sequence G-G-G-G-(A)20-C-C-C-C, where 20 adenosine bases form the loop region and the G-C base pairs form the stem of the MB. This MB is coupled to a small peptide sequence that contains a disulphide bridge in spatial close proximity to a Trp residue (peptide sequence: KAMHAWGCGGGC-NH2 where CGGGC is cyclic, i.e. it is closed with a disulphide bridge between the two cysteine (C) residues). The molecular mass of this peptide is ~1175 g/mole. The peptide is coupled to one of the strands of the stem of the molecular beacon. In one strand of the stem, there is an attached fluorophore (Cy3) which is quenched by DABCYL, located on the other strand of the stem.

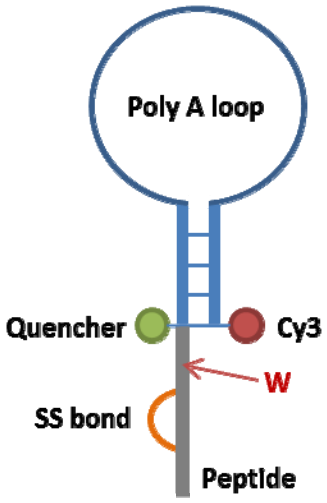

Figure 2. Molecular Beacon construct. The peptide linked to the MB has a disulphide bond (SS bond) nearby a Trp (W) residue. The presence of a quencher nearby the fluorophore Cy3 is responsible for the low fluorescence emission intensity of the closed form the MB.

2.2.1 C-reactive protein

C- reactive protein is a protein that has been the subject of interest to research due to its increased presence in cases of injury or infection[16]. It presents a pentameric structure with each protomer composed of 206 amino acid residues. The 3D structure of the protein is diplayed in Figure 3. Each protomer contains 6 Trp residues, 8 Tyr residues and 1 disulphide bridge. Since Trp and Tyr residues can be found in such close spatial proximity to the disulphide bridge in the protomer, CRP is a very good candidate for LAMI. The crystallographic data used for the display of the 3D protein structure (Figure 3) was retrieved from RCSB Protein Data Base (PDB) (1GNH.pdb). The structure has been displayed using Discovery Studio 4.5 (Accelrys Software, San Diego, CA, USA). Distances between Trp, Tyr and Cys residues are displayed in Figure 3.

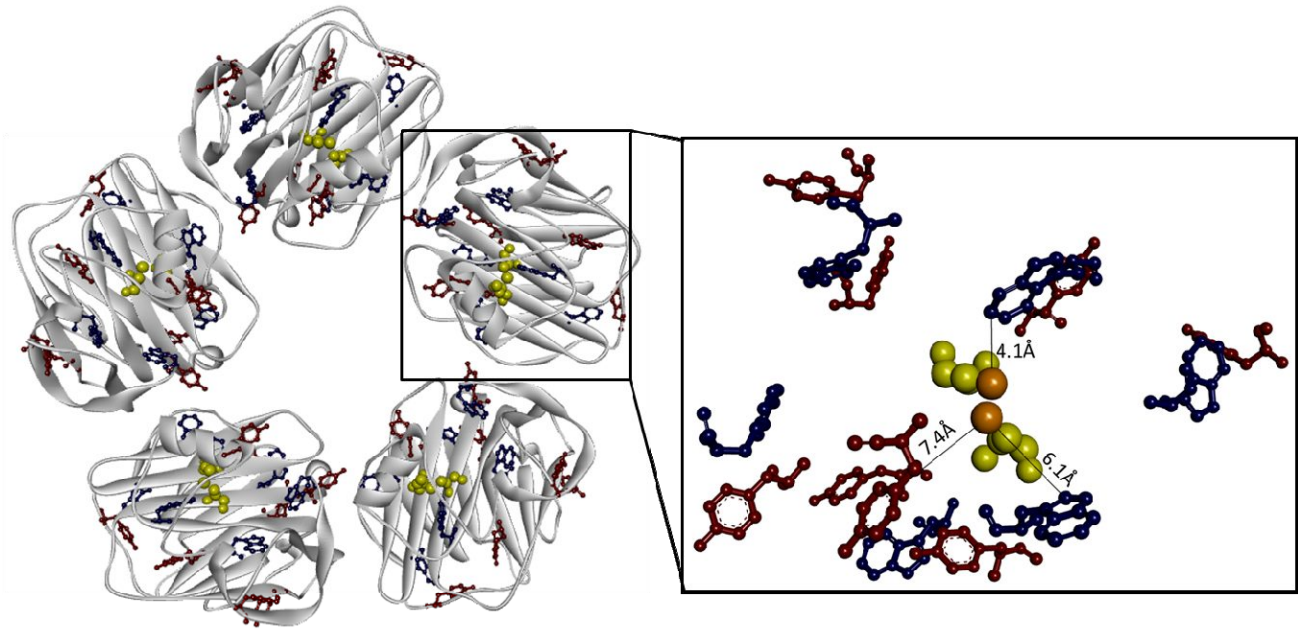

Figure 3. CRP 3D molecular structure, according to 1GNH.pdb. Protein backbone is displayed in grey, Trp residues in blue, Tyr residues in red and Cys in yellow. Insert: zoom into the structure. Sulfur atoms on the Cys residues are displayed in orange. The distances between these sulfur atoms and the closest nearby Trp and Tyr residues are also displayed: the distance between Cys36(SG) -Trp162(CH2) is 4.1Å; the distance between Cys97(SG) –Trp110(CD1) is 6.1Å; the distance between Cys97(SG)-Tyr175 (CG) is 7.4Å.

2.3. Slide preparation

Optically flat quartz slides were purchased from ArrayIt (SuperClean 2, SCM2). The slides were placed in a hydroxylating solution (200 ml ionized/destilled water + 10.0g $K_2S_2O_8$) at ~99^0C for 60 min. The hydroxylation solution was then replaced by deonised water (to avoid salt formation on the surfaces). The surfaces were then cleaned with pure water and were dried using compressed dry air. Subsequently, the surfaces were coated with a thiol based linker by submerging them in a solution of 0.3% v/v 3-mercaptopropyl-trimethoxysilane in m-xylene for 30 min. The surfaces were then removed from this solution and flushed with pure xylene, 70% ethanol and deonized water and finally dried with compressed dry air. Subsequently, the surfaces were placed in an oven at 100^0C for 60 min.

2.4. Illumination setup

A schematic of the experimental system designed and built in collaboration between Newport Corporation's Technology and Applications Center (TAC) and Aalborg University, Denmark, is shown in Figures 4 and 5.

2.4.1 One-photon UV optical setup

The laser light source is a Tsunami XP (Spectra-Physics) pumped with the Millennia eV (Spectra-Physics). The Tsunami femtosecond laser source is manually tunable from 700-1080nm with ~100fs pulse width and a repetition rate of 80MHz. Typical operation wavelength is around 840nm with a max average power of 3W. The output of the Tsunami is frequency tripled in a UGH module (Spectra-Physics) to produce ~280nm UV femtosecond pulses at 80MHz with an efficiency of ~10%. The fundamental at 840nm and the third harmonic at 280nm are routed via separate paths into the experimental system. Each beam passes through a computer controlled variable attenuator consisting of a half-wave plate, mounted in a motorized rotation stage (PR50CC, Newport), and followed by a polarizing beam cube. After each attenuator a fused silica beam sampler is used to direct a portion of the beam onto a photodiode (PD-300R-3W and PD-300R-UV, OPHIR) for power monitoring. The beams then passes through safety shutters (LS6S2ZM1, VINCENT ASSOCIATES) to control exposure to the sample.

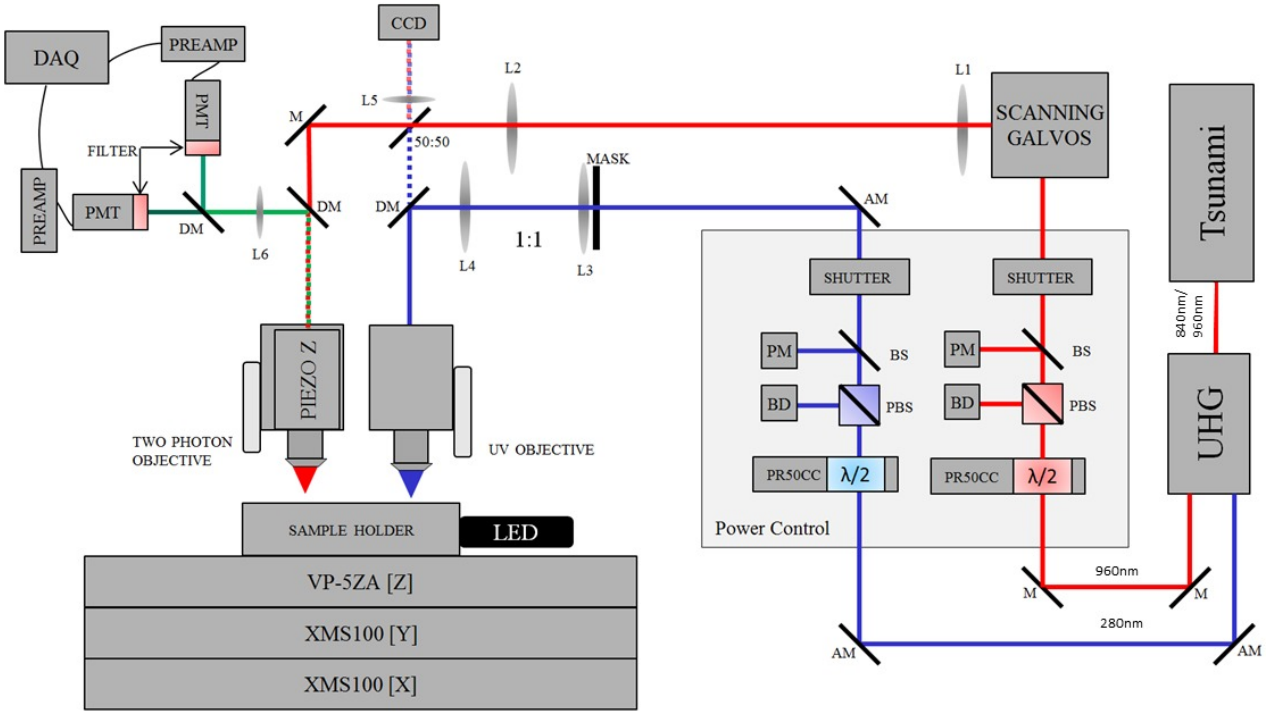

Figure 4. Experimental Layout. AM: Aluminum Mirror; M: Mirror; λ/2: Half Wave Plate; PBS: Polarizing Beam Splitter; BD: Beam Dump; BS: Beam Sampler; PM: Power Meter; L1: Scan Lens; L2: Tube Lens; 50:50: Beam Splitter; DM: Dichroic Mirror; L3,L4: Relay Lens; L5: Tube Lens; L6: Concentrator; DAQ: Data Acquisition Card; PREAMP: preamplifiers; PMT: Photon multiplication tube.

2.4.2 Two-photon microscope

A 960nm beam is used to generate two or three-photon epifluorescence from a sample placed under a 40X Olympus UPLFLN Objective 0.75NA, 0.51mm WD. The objective used for multi-photon generation is mounted on a piezo actuated stage with a range of 250µm (NPO250SG-D, NEWPORT) for precision control in Z. The fluorescent image is formed by raster scanning the 960nm beam using an XY galvo assembly (Cambridge Technologies - 6215H) along with a scan lens and tube lens configuration. The back propagating epifluorescence signal is directed towards a detection setup using a dichroic mirror, transparent at 840nm and reflective for shorter wavelengths. The epifluorescence passes through a filter, to block any remaining fundamental, and a concentrating lens to focus the light onto the active area of two separate PMTs (H10770PA-40, HAMAMATSU). The two PMT's are separated by another dichroic to allow imaging reconstruction at different florescent wavelengths. The PMT's are powered by a low voltage power supply (PS-2/LV, SUTTER) with variable gain. Their signals first pass through low noise preamplifiers (XPG-ADC, SUTTER) positioned close to the PMT's to reduce unwanted noise. Signal acquisition is accomplished using a PCI DAQ card and breakout box (PCI-6110 S SERIES, BNC-2110, National Instruments). The analog outputs from this card are used to control the position of the galvo scanning mirrors. Previous work has gone into greater depth on two photo microscope design and implementation .

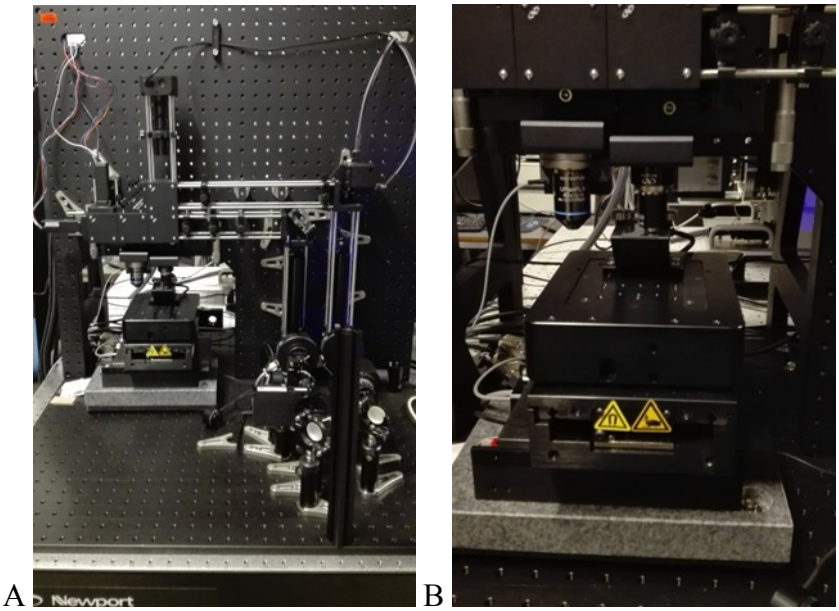

Figure 5. Photographs of the custom microscope and microfabrication stage (A) and zoomed region (B) displaying the microfabrication stage with the sample holder and the UV (right) and IR (left) objectives. Please see the total description of the optical setup in Figure 4.

2.4.3 Moving Stage, Objectives and CCD camera

The 280nm beam is used to generate a diffraction pattern at the focal plane of a UV objective (LMU-40X-UVB, THORLABS). In order to define the diffraction pattern formed, the beam passes through an aperture mask and a 1:1 telescope before being directed into the UV objective with a dichroic. The dichroic is reflective below 310nm and transmits longer wavelengths.

To simplify positioning of the sample a custom holder was provided to allow transmitted LED illumination (LCS-0420-03-22, LCS-0850-03-22, MIGHTEX). LED illumination transmits through the system from either objective onto a single windowless CCD (MCE-B013-UW, MIGHTEX). Using a windowless CCD allows imaging UV light that would otherwise be absorbed in the protective glass cover typical on most CCDs. A fused silica lens is used to form an image of the sample on the CCD. The imaging lens is fused silica to allow 280nm light to reach the CCD in order to view the diffraction pattern being formed. Both objectives are mounted on manual 25mm linear stages for course alignment. The UV objective and the multi-photon objective are positioned very close to each other to allow minimal sample translation between both channels. The sample holder is mounted to an XYZ stage stack comprised of two XMS100 stages (XY) and one VP-5ZA (Z). All stages, including the rotation stages for power control, the piezo Z stage for fine positioning, and the XYZ stack, are controlled with the Newport XPS-Q8 motion controller with appropriate driver cards. Typically a sample is prepared for exposure to a diffraction pattern generated with the UV source. After exposure to the UV source the sample is then translated to the focal region of the two-photon microscope for imaging/analysis.

2.4.4 Microfabrication software

The Microfabrication stage is controled through an interface software. In Figure 6 is displayed a screen shot of the software and the features which can be controled. On the lower left panel is a 3D view of the pattern (array) according to which the biomolecules shall be illuminated. The desired uploaded bitmap will be displayed in a 2D or 3D view, as exemplified with an array pattern, in the lower left panel in Figure 6. The software also allows the control of the velocity and acceleration of the stage movement as well as a controlled XYZ start position offset. The movement of the stage will be coordenated with the opening of the shutter, according to the set velocity and acceleration of the moving stage. The light power passing through the objective can be controled as well. On the right panel displayed in Figure 6, a real time

imaging of the samples can be visualised by the CCD camera installed above the objectives (see Figures 4 and 5A). The LED used to illuminate the sample can also be controled through the software.

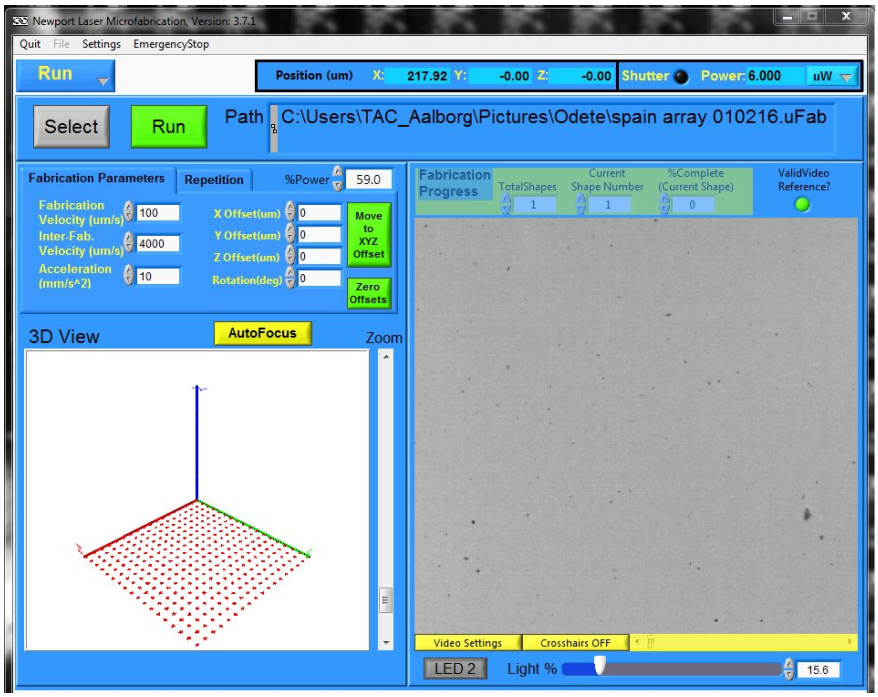

Figure 6. Screen shot of the interface software that controls the microfabrication stage.

2.5 Molecular immobilization

A 1µL droplet of the sample solution (protein or MB) was placed on the surface of the optically flat SH derivatized slide. After the droplet was dried at room temperature, the sample was placed in the sample holder of the illumination setup. The samples were illuminated at 280nm according to an array pattern (500x500µm, bitmap image) uploaded to the stage controling software. Illumination was performed at a speed of 100µm/s with a focused laser beam. The average pitch distance (distance between the center of neighbouring spots) was 30µm and the illumination power varied according to the samples (60µW for CRP and 20µW for MB). After illumination, samples were washed overnight with 1xPBS buffer plus 0.1% Tween 20 detergent and rinsed with PBS 1x. The slides were then scanned on a fluorescence confocal microscope (LEICA TCS SP5) with a HeNe laser for CRP (633nm excitation line) and for MB (543nm excitation line).

2.5.1. MB binding Immunoassay

The immobilized MB array was incubated with the complementary poly T oligonucleotide for 90min at 37˚C. After incubation, the slides were washed with PBS 1x plus 0.1% Tween 20 detergent followed by PBS 1x. The slides were then scanned on a fluorescence confocal microscope (LEICA TCS SP5) with a 543nm excitation light. Enhanced fluorescence of the MB-complementary oligonucleotide hybrid was compared to the poorly fluorescent MB. The detection scheme for the immobilized MB-complementary oligonucleotide hybrid is depicted in Figure 7.

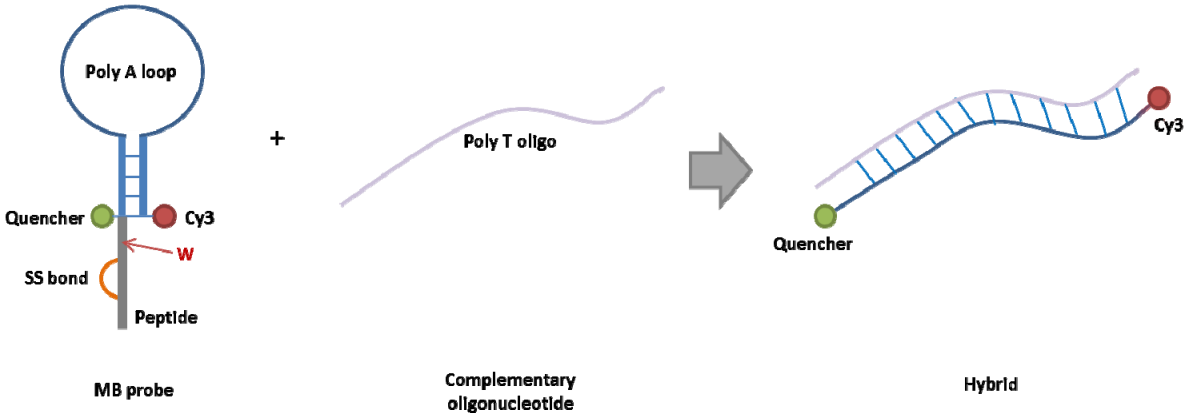

Figure 7. Molecular detection mechanism. The MB containing a poly A loop will hybridize with the complementary poly T oligonucleotide, opening the loop. The Cy3 fluorescent probe will no longer be quenched by DABCYL and there will be an increase in fluorescence intensity.

2.5 Array Imaging

The arrays were visualized with an inverted confocal fluorescence microscope (LEICA TCS SP5). Cy3 fluorophore present in the MB was excited using the 543nm laser line form the HeNe laser and Alexa Fluor 647 present in the CRP was excited using the 633nm laser line from the HeNe laser. Both samples were visualized through an UV 20x objective.

2.6 Microbeads imaging with 2-photon microscopy

Fluorescent Carboxyl Polymer Particles (P(S/5%MAA/5.5%DVB), catalog number FC05F, labeled with Dragon Green·(excitation wavelength:480nm; emission wavelength: 520nm) were purchased from Bangs Laboratories, Inc., USA. The microbeads (4.95µm) were excited at 960nm from the fundamental output, which generated 2-photon epifluorescence (480nm). An average of 600 images were obtained and superimposed, resulting in a higher resolution image of the microbeads (Figure 13).

2.7 Data analysis

ImageJ 1.50i was used to obtain the fluorescence emission intensity profiles and the 3D surface plot of the CRP and MB arrays imaged by confocal fluorescence microscopy. For the intensity profiles, a portion of the image was selected and analysed. For the 3D surface plot, the array area was selected and analysed, adjusting the lighting, the perspective and the smoothing. MATLAB v7.1 SP3 was used to develop a versatile software package (BNIP-Pro) that allows for advanced analysis of the protein array images.

3. RESULTS AND DISCUSSION

3.1 CRP array immobilized with LAMI

In Figure 8A is depicted a 500x500µm array where the spots display 30µm pitch distance (distance between the centre of neighbouring spots). A 3D surface plot of the array is shown is Figure 8B where it is possible to observe a good spatial resolution between spots. This can also be observed by the intensity profile analysis displayed in Figure 8. There is a high uniformity of peaks across the profile and the signal to noise ratio is low.

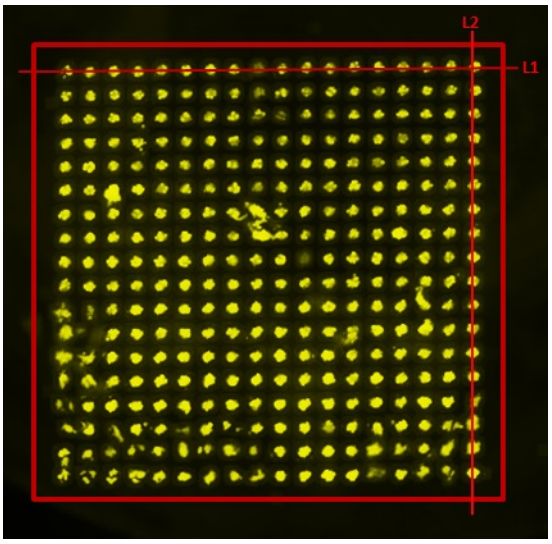

A

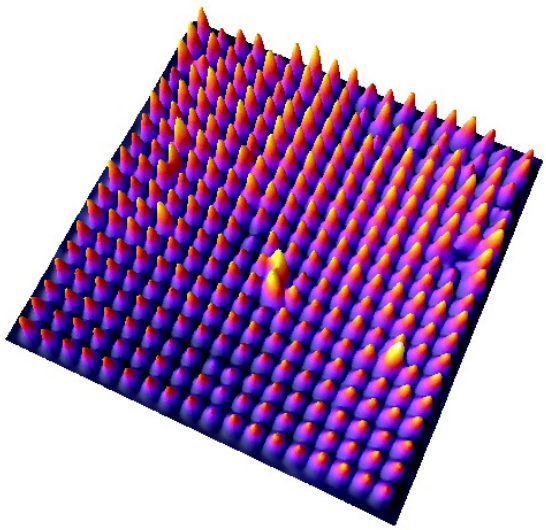

B

Horizontal fluorescence emission intensity profile along L1

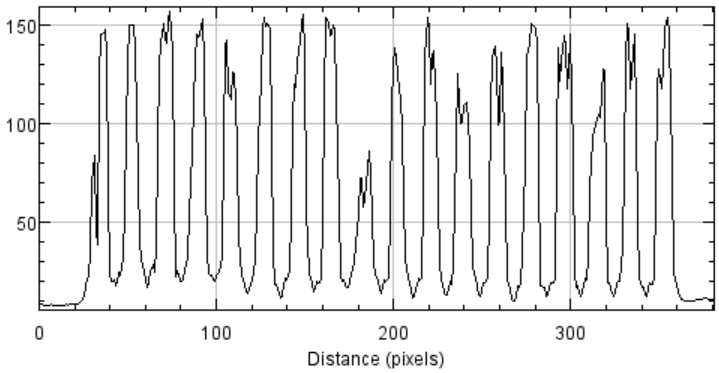

C

Vertical fluorescence emission intensity profile along L2

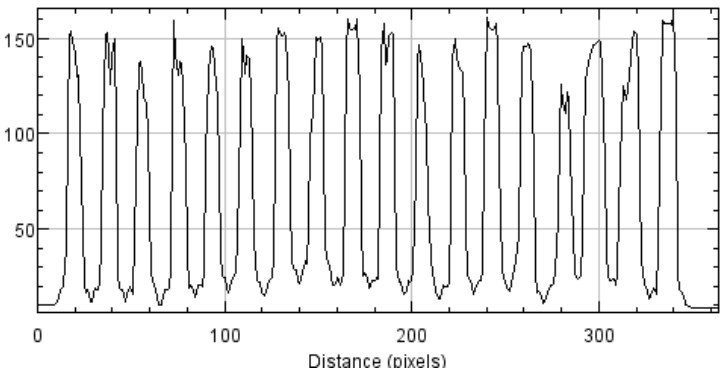

D

Average fluorescence emission intensity profile of the whole array (red line)

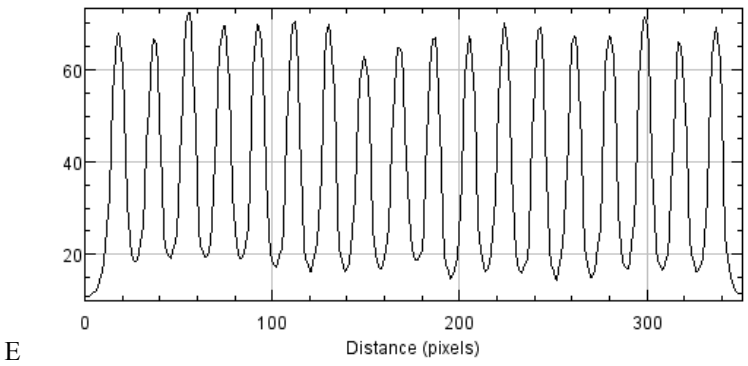

E

Figure 8. CRP array analysis. A- Confocal fluorescence image of CRP immobilized according to an array; B- Three dimensional surface plot representation of the immobilized protein arrays. C- Fluorescence emission intensity profile along line L1 of the immobilized CRP array; D- Fluorescence emission intensity profile along line L2 of the immobilized CRP array; E- Fluorescence emission average intensity profile of the whole array (red square).

Further processing of the original acquired images was performed in order to enhance the array features. The methods used involved Fourier transformation of the original image and selection of the most intense Fourier peaks after which the resulting Fourier map was transformed back to the spatial dimension. In figure 9 it is possible to observe the original images and the images obtained after FFT processing.

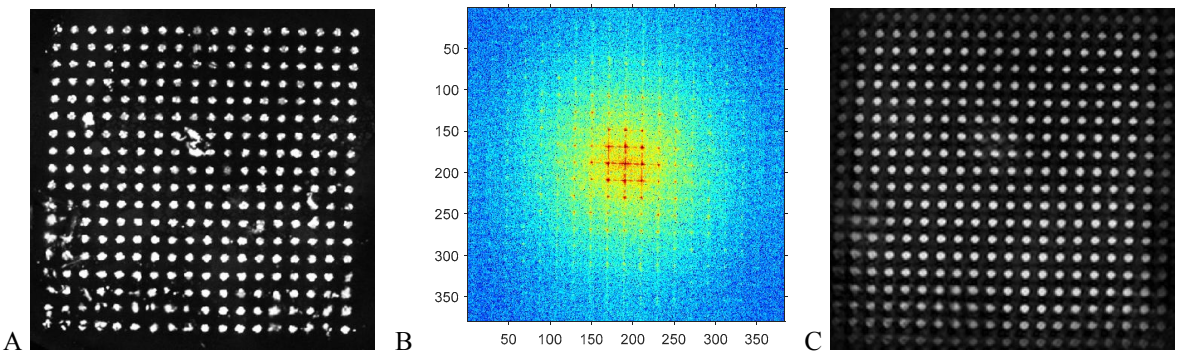

A B C

Figure 9. Fourier analysis of the CRP array. A- Original images of the CRP array on a grey scale; B – 2D Fourier transform of the CRP array (A); C – Fourier map, transformed to the spatial dimension, of the original images of the CRP array (A).

The artefacts observed in the original image (Figure 9A) disappear because only periodic features are selected from the 2D map (Figure 9B), since we select only the most intense peaks in the 2D Fourier map. The Fourier transformed images show a periodic distribution which can be attributed to each spot in the array. The spots observed at the edges of the processed FFT image (Figure 9C) are echoes of the most intense peaks selected in the FFT map (Figure 9B) and should be disregarded.

A statistical analysis of some features of the CRP array was also performed. The histograms of the peak intensity and variance distribution, intensity maximum distribution and of the area distribution of the peaks in the array are displayed in Figure 10. Each spot was characterized as a peak and a cut-off of 0.5 was selected to exclude the background signal. It is possible to observe that the maximum intensity distribution in the array is approximately one for all peaks (Figure 10C). This means that very sharp and defined peaks were obtained which correlates to the well-defined array visualized. Also, it can be observed that the area of these peaks is mostly distributed into a single curve, which correlates well with what is observed in the array, where defined and independent spots are seen. Although these curves do not present a perfect Gaussian shape (Figure10A and 10B, where the mean fluorescence intensity distribution of all peaks and the

variance of such values are displayed, respectively), it can be concluded that the area distribution of each spot is fairly even. For the area distribution, a column is displayed with a value around zero (Figure 10D). This column must be associated with some artefacts and background noise found in the array that was above the chosen cut-off. The mean distribution of the intensity of each peak (Figure 10A) also correlates well with the observed results. In the original array image, each spot presents a brighter point in the centre where the fluorescence intensity is higher and then the intensity decreases in the outer rim of each spot. This translates well to the data depicted in the histogram relatively to mean distribution of each peak's intensity (Figure 10A).

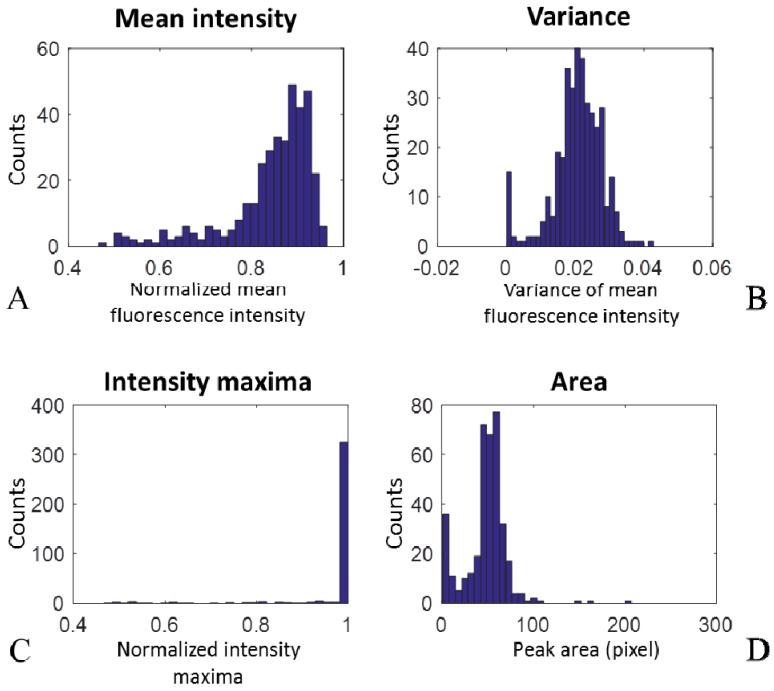

Figure 10. Histograms of the normalized peak intensity distribution (A), variance of intensity distribution (B), normalized intensity maximum distribution (C) and of the area distribution of the peaks (D) in the array.

In Figure 11 is displayed the analysis of the signal to noise (S/N) ratio for the CRP array. In the upper right corner the original array is displayed (array to the left) and each spot is identified by a green outer rim. Such spots are then isolated and displayed on the array to the right. Those points can then be subtracted from the original image to obtain the background (lower left array). This will allow the analysis of the S/N to noise ratio. This analysis is plotted on the left. The S/N ratio is approximately 75 with a confidence interval of ± 25. Some outliers can also be found outside the confidence interval. Nevertheless, there is a reasonable S/N distribution.

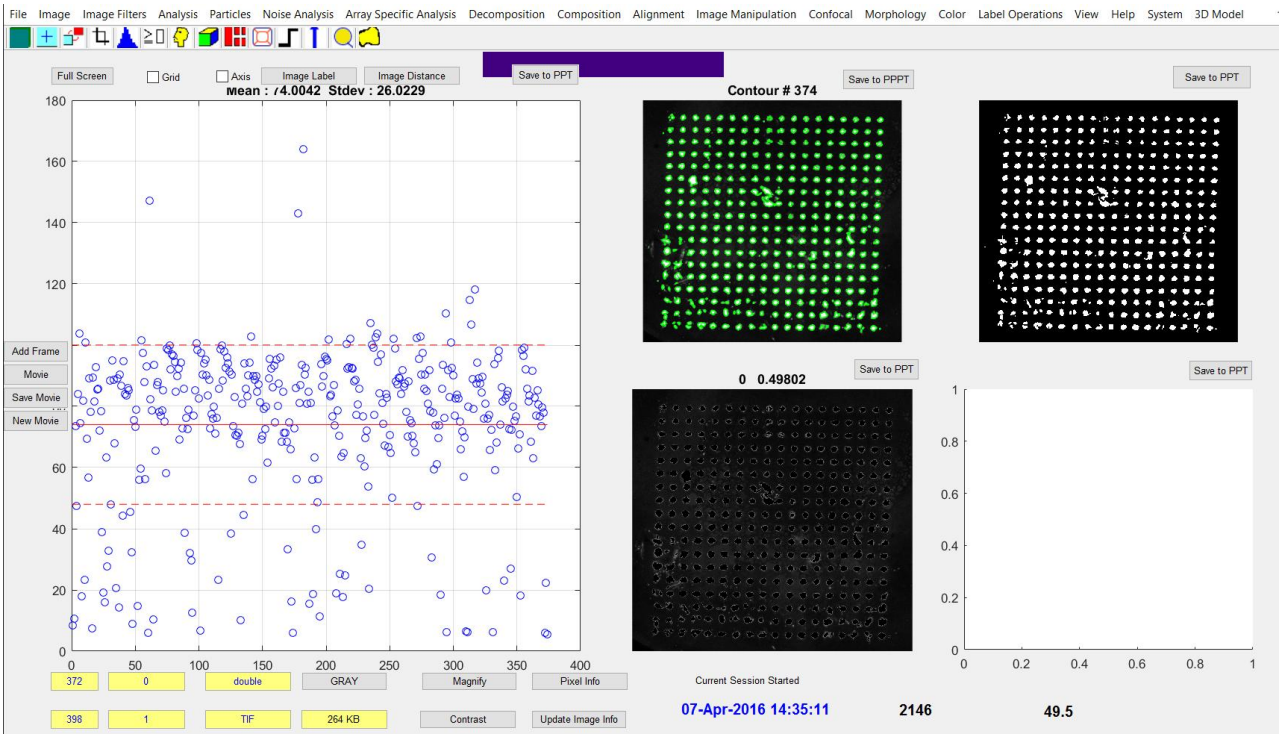

Figure 11. Graphic User Interface (GUI) displaying the analysis of signal to noise (S/N) ratio on the CRP array. In the upper left panel, the peaks in the array are identified and marked. These peaks are subsequently isolated from the background (upper right panel) and are then subtracted from the original image in order to calculate the noise level around the peaks in the array (left lower panel).

3.2 MB array immobilized with LAMI followed by molecular recognition of complementary oligonucleotide

In Figure 12 is depicted a confocal fluorescence image of a 500x500µm array of immobilized MB before (Figure 12A) and after hybridization with the complementary oligonucleotide (Figure 12B). The low fluorescence emission intensity displayed by the array in Figure 12B is to be expected since in the design of our model MB, there is a quenching molecule (DABCYL) placed nearby the fluorescent molecule (Cy3). However, a signal can still be detected, which corresponds to a successful immobilization of the MB. After hybridizing the immobilized MB, the fluorescence intensity increases significantly, as it can be observed in Figure 12B.

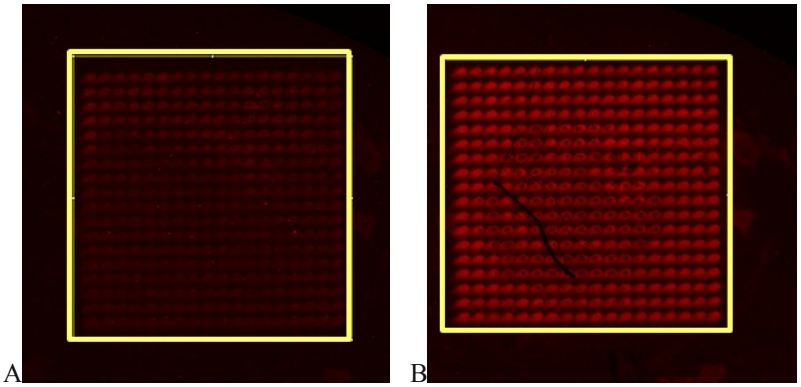

A B

Average fluorescence emission intensity profile of the whole array to the left (A)

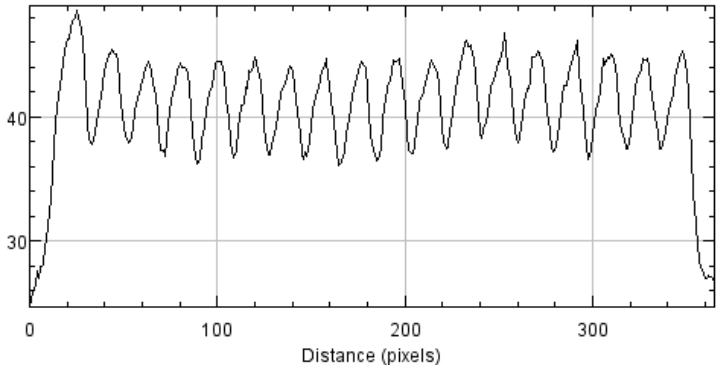

C

Average fluorescence emission intensity profile of the whole array to the left (B)

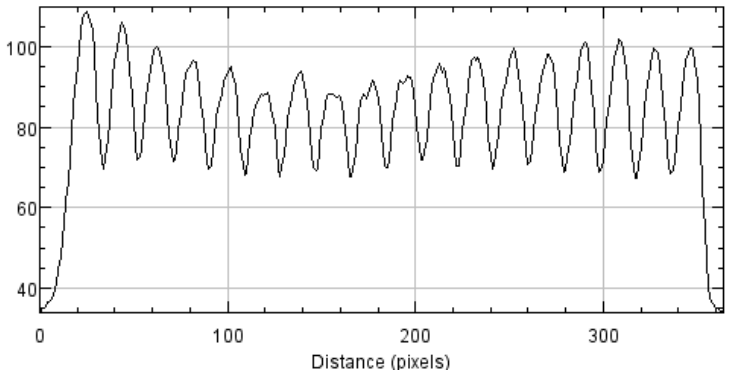

D

Figure 12. Fluorescence confocal images of an immobilized MB array and analysis of the average fluorescence emission intensity profiles. A- Fluorescence emission intensity of the array prior to hybridization with complementary oligonucleotide. B- Fluorescence emission intensity of the MB array after hybridization with complementary poly-T oligonucleotide. C- Average fluorescence emission intensity profile of the immobilized array in (A) under the selected area (yellow Square). D- Average intensity profile of the immobilized array in (B) under the selected area (yellow Square).

This is coherent with our predicted detection mechanism displayed in Figure 7. After hybridization with the complementary oligonucleotide (poly T), the poly A loop of the MB opens and Cy3 is no longer in spatial close proximity to the quencher, increasing the fluorescence signal. The successful hybridization can also be corroborated with

the average profile analysis of the immobilized array after and before hybridization (Figure 12). An increase in the intensity of the average profile of the array after hybridization (Figure 12D) is registered.

These results also show that the illumination leading to the immobilization of the MB did not affect the biorecognition capacity of the MB. If the oligonucleotide loop present in the MB had been structurally damaged, hybridization with the complementary oligonucleotide would not occur, which is not the case. Furthermore, our data also shows that the coupling of a small peptide to the MB, containing a disulphide bridge and a tryptophan in close spatial proximity, mimicking what is found in nature, is a viable and good strategy in order to apply LAMI to achieve immobilization of various kinds of biosensors.

3.3 Imaging with microfabrication stage

The new microfabrication stage also allows for imaging structures in the micrometer range with an integrated two-photon microscope. A single image of the microbeads has been acquired in 0.3s. 25 of such images were acquired and the average low signal to noise image is displayed in Figure 13A. Afterwards, 600 of such images were collected and drift corrected prior to superimposition. The drift corrected high resolution image is displayed Figure 13B.

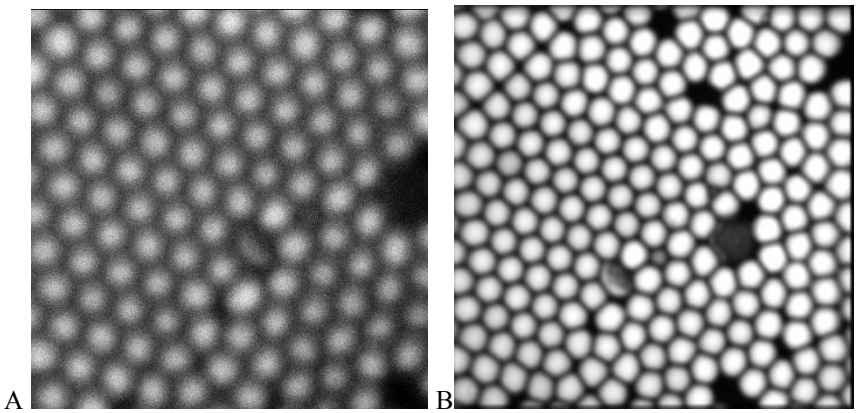

Figure 13. Imaging fluorescent microbeads (4.95 micrometer in diameter) with the stage integrated two-photon microscope. A- Poor signal to noise image obtained as the average of 25 non-drift corrected images. B- High resolution image obtained by superimposing 600 drift corrected images.

The diameter of the microbeads is 4.95 micrometer. The resolution in the superimposed high resolution image is at least at the diffraction limit, which with the present objective and fluorescence wavelength 300 nm.

4. CONCLUSION

The illumination setup reported in this paper is novel and allows for one- and multi-photon LAMI. Furthermore it can also be used as a multi-photon microscope with imaging capabilities. It allows for the visualization of light diffraction patterns formed by spatial masks. In this proceeding paper, we report some of the early results obtained with this new setup and the whole range of possible applications is currently being developed.

5. ACKNOWLEDGMENTS

The authors acknowledge the funding from the European Commission through the project H2020-644242 –SAPHELY and the project H2020-634013-2-PHOCNOSIS. The authors also would like to acknowledge Miguel Ángel González Martínez and Maria Jose Bañuls from Universitat Politècnica de València (UPV).

6. REFERENCES

[1] Sassolas, A., Blum, L. J. and Leca-Bouvier, B. D., "Immobilization strategies to develop enzymatic biosensors," Biotechnol. Adv. **30**(3), 489–511 (2012).

[2] Jonkheijm, P., Weinrich, D., Schröder, H., Niemeyer, C. M. and Waldmann, H., "Chemical strategies for generating protein biochips," Angew. Chemie - Int. Ed. **47**(50), 9618–9647 (2008).

[3] Bent, D. V. and Hayon, E., "Excited state chemistry of aromatic amino acids and related peptides. III. Tryptophan," J. Am. Chem. Soc. **97**(10), 2612–2619 (1975).

[4] Duroux, M., Skovsen, E., Neves-Petersen, M. T., Duroux, L., Gurevich, L. and Petersen, S. B., "Light-induced immobilisation of biomolecules as an attractive alternative to microdroplet dispensing-based arraying technologies," Proteomics **7**(19), 3491–3499 (2007).

[5] Petersen, S. B., di Gennaro, A. K., Neves-Petersen, M. T., Skovsen, E. and Parracino, A., "Immobilization of biomolecules onto surfaces according to ultraviolet light diffraction patterns.," Appl. Opt. **49**(28), 5344–5350 (2010).

[6] Skovsen, E., Kold, A. B., Neves-Petersen, M. T. and Petersen, S. B., "Photonic immobilization of high-density protein arrays using Fourier optics," Proteomics **9**(15), 3945–3948 (2009).

[7] Petersen, M. T., Jonson, P. H. and Petersen, S. B., "Amino acid neighbours and detailed conformational analysis of cysteines in proteins.," Protein Eng. **12**(7), 535–548 (1999).

[8] Neves-Petersen, M. T., Snabe, T., Klitgaard, S., Duroux, M. and Petersen, S. B., "Photonic activation of disulfide bridges achieves oriented protein immobilization on biosensor surfaces.," Protein Sci. **15**(2), 343–351 (2006).

[9] Neves-Petersen, M. T., Gajula, G. P.and Petersen, S. B., "UV Light Effects on Proteins : From Photochemistry to Nanomedicine," Mol. Photochem. - Var. Asp., 125–158 (2012).

[10] Neves-Petersen, M. T., Gryczynski, Z., Lakowicz, J., Fojan, P., Pedersen, S., Petersen, E. and Petersen, S. B., "High probability of disrupting a disulphide bridge mediated by an endogenous excited tryptophan residue.," Protein Sci. **11**(3), 588–600 (2002).

[11] Parracino, A., Gajula, G. P., di Gennaro, A. K., Correia, M., Neves-Petersen, M. T., Rafaelsen, J. and Petersen, S. B., "Photonic immobilization of bsa for nanobiomedical applications: Creation of high density microarrays and superparamagnetic bioconjugates," Biotechnol. Bioeng. **108**(5), 999–1010 (2011).

[12] Correia, M., Neves-Petersen, M. T., Jeppesen, P. B., Gregersen, S. and Petersen, S. B., "UV-light exposure of insulin: pharmaceutical implications upon covalent insulin dityrosine dimerization and disulphide bond photolysis.," PLoS One **7**(12), e50733 (2012).

[13] Correia, M., Neves-Petersen, M. T., Parracino, A., di Gennaro, A. K. and Petersen, S. B., "Photophysics, photochemistry and energetics of UV light induced disulphide bridge disruption in apo-α-lactalbumin," J. Fluoresc. **22**(1), 323–337 (2012).

[14] Correia, M., Snabe, T., Thiagarajan, V., Petersen, S. B., Campos, S. R. R., Baptista, A. M.. and Neves-Petersen, M. T., "Photonic Activation of Plasminogen Induced by Low Dose UVB," PLoS One **10**(1), e0116737 (2015).

[15] Parracino, A., Neves-Petersen, M. T., Di Gennaro, A. K., Pettersson, K., Lövgren, T. and Petersen, S. B., "Arraying prostate specific antigen PSA and Fab anti-PSA using light-assisted molecular immobilization technology," Protein Sci. **19**(9), 1751–1759 (2010).

[16] Shrive, A. K., Cheetham, G. M., Holden, D., Myles, D. A. A., Turnell, W. G., Volanakis, J. E., Pepys, M. B., Bloomer, A. C. and Greenhough, T. J., "Three dimensional structure of human C-reactive protein.," Nat. Struct. Biol. **3**(4), 346–354 (1996).